Proceedings of the ASME 2019 38th International Conference on Ocean, Offshore and Arctic Engineering
OMAE2019
June 9-14, 2019, Glasgow, Scotland, UK

OMAE2019-95798

HYDRODYNAMIC MODELLING AND ESTIMATING RESPONSE OF GLACIAL ICE NEAR A DRILLING RIG

Babak Ommani*
SINTEF Ocean,
Centre for Autonomous Marine Operations and Systems (AMOS), NTNU,
Trondheim, Norway
*babak.ommani@sintef.no

Petter Andreas Berthelsen
Halvor Lie
Vegard Aksnes
SINTEF Ocean,
Trondheim, Norway

Geir Løland
Petroleum Safety Authority,
Stavanger, Norway

ABSTRACT

Impact scenarios involving a typical drilling rig and glacial ice are studied. The goal is to better identify the important physical effects in modelling the dynamics of glacial ice in presence of waves and a floating platform, whilst improving simulation tools to capture the location and energy of possible collisions. A state-of-the-art numerical model of a typical semi-submersible is developed and calibrated with model tests to represent the drilling rig. A systematic incremental approach is adopted to model the dynamics of glacial ice. Long wave approximation, nonlinear excitation and restoring forces, interaction forces with the semi-submersible, and viscous forces due to flow separation are among the models which are considered step by step. The sensitivity of the resulted collision scenario to the modelling choices is investigated. The possibility of impact with columns, pontoons, and risers are particularly studied. Based on the obtained results, recommendations are made for modelling of glacial ice dynamics in presence of a floating platform.

INTRODUCTION

Taking proper and timely measures to avoid ice interactions with floating units is a key part of ice management procedures. These measures may include temporary relocation of the floating unit, if possible and necessary. Growlers and bergy bits, created by ice detachment from the edge of a glacier, can be difficult to detect visually or by radar. Therefore, the consequences of a possible impact between these smaller ice masses and floater units need to be assessed.

Sayeed et al. [1] present a comprehensive review on the literature related to hydrodynamic interaction between drifting ice and offshore structures for the past 30-40 years. In their review, they categorize the problem of drifting ice trajectory and impact with structures into three phases: far-field, near-field and contact phases. A short summary of the main findings is presented here; focusing on the hydrodynamics in the far field and near field phases.

In the far-field region, the objective has been to accurately predict the trajectory of drifting ice. Drift models in open water have been studied. Statistical models that rely on the past trajectories to predict future paths have also been applied. Most of the work has been focused on the larger icebergs, and some of the discussions have been related to the importance of including wave forces for better prediction of the drift trajectories. For smaller bergy bits, the drift trajectories will be more affected by waves and surface current than deep current. Furthermore, the drift models assumed a constant added mass which is not valid for ice masses close to large offshore structures [2].

In iceberg impact analysis, models which include only mean drift speed have shown to underestimate the impact velocity. This is even more pronounced for smaller icebergs. Several studies were conducted on wave induced motions of smaller ice fragments. For example, in [3, 4] the authors applied linear potential-flow theory to calculate wave induced surge and heave responses. It was also demonstrated by [4] that smaller icebergs show fluid particle motion behavior for wave length to iceberg ratios greater than 10-15. This was later confirmed by experimental results [5] where the ratio was 13. Many of the studies demonstrated the increasing importance of wave-induced motions as the size of the ice mass decreases. The shape of the iceberg was also shown to be important in some cases for the total surge velocities [6].

The effect of a large offshore structure presence received more attention in the near field analysis (e.g. [7, 8]). The study in [8] showed that the zero-frequency added mass increases prior to impact, but exclusion of viscous effects as well as coarse discretization of the numerical model deemed the results unreliable. Isaacson and McTaggert [9] found that the added mass varies with impact duration. It was suggested to use infinite-frequency added mass for short duration and zero-frequency added mass for longer impact durations. Furthermore, the presence of the structure can result in velocity reduction. For relatively small icebergs (diameter ratio of less than 0.5 compared to structure), the repellent forces may lead to significant reduction of impact velocity and in some cases no collision. Similarly, the hydrodynamic

interaction was concluded to reduce the approaching velocity in [10, 11]. LS-DYNA was used to investigate effect of sea water in a fluid-structure interaction in [12] for iceberg approaching a LNGC. It was found that the pressure increased drastically due to the confined water layer entrapped between the two bodies as the ice mass approached the hull. However, for slowly approaching icebergs the water between the two bodies will have time to flow away without resistance and the same pressure increase will not be present.

The near field problem has also been investigated through various physical model tests [5, 13, 14] in order to assess the effects of iceberg size and shape. The ratio between wave length (λ) and the characteristic length (L) of the iceberg dictates if the iceberg shows particle-like motion or not. For long waves, with λ/L larger than 13, [5] found the iceberg to behave like particles, while diffraction and viscous effects were important when λ/L was less than 10. For ratios between 10 and 13, the iceberg motion was dependent on its shape. The influence of iceberg size relative to structure size was investigated by [13, 15] and no collisions were found to occur if the iceberg was small enough, that is, the characteristic length of the iceberg was less than 0.2-0.5 times the structure size (diameter in case of a column or cylinder). For medium sized icebergs, [13] found eccentric collisions and sometimes repetitive collisions.

The contact phase is usually modelled separately from the near field phase. There are several challenges related to the contact phase, but only the hydrodynamic ones are highlighted here. The added mass of ice and structure, as well as associated coupling terms are needed for computation of impact energy. A common assumption is to use a constant added mass of 0.5 times the ice mass for the ice [16, 17, 18, 19], although several studies [20, 19] show that the impact load is sensitive to this uncertain added mass value.

The Norwegian Petroleum Safety Authority has identified knowledge gaps for safe operation of floating units related to impact with smaller glacier ice masses. An earlier study [21] showed that semisubmersible drilling units may not withstand impacts from smaller ice masses, i.e. 15m characteristic length and smaller, even if they are reinforced to withstand ship collisions. The study shows that the ice can hit both above and below areas reinforced for ship collisions. Furthermore, it can pass through the columns and potentially hit the drilling riser. Two different modelling approaches are used to quantify the hydrodynamic characteristics of ice masses. The main part of the study is based on linearized frequency domain analysis applied to calculate the wave frequency relative motion between the ice and the drilling unit. Impact area and energy was estimated from the extreme value statistics assuming the impact to be a narrow banded stochastic process. The second adopted method was a nonlinear time domain analysis, where the objective was to investigate nonlinear hydrodynamic effects on a single ice piece (without the interaction of the drilling unit). The findings from this study include:

- Multibody analysis in frequency domain showed that the wave frequency response of glacial ice masses is affected by the presence of a drilling unit, but not vice versa.
- There are uncertainties related to damping in heave, roll and pitch.
- The nonlinear time domain analysis showed substantially larger pitch motions than the linear frequency domain analysis.

In the present study, the response of ice in waves is further investigated using time-domain simulations and by partly introducing important nonlinear effects. This includes:

- Adopting a 6-degree of freedom simulation in time-domain, which better accounts for the role of stochastic variability of waves on impact and allows for introducing quadratic forces.
- Introducing viscous drag forces using Morison-type elements.
- Accounting for nonlinear Froude-Krylov and buoyancy forces.
- Investigating the hydrodynamic interaction between ice and platform.
- Perform sensitivity study on impact scenario to ice initial location and wave realization.
- Briefly studying the repellent force introduced by variation of zero-frequency added mass as the ice gets closer to the platform.

PROBLEM DEFINITION AND MODELS

Motions of glacial ice in presence of a typical drilling rig in a selection of environments are studied here numerically. The problem involves a dynamic model for the drilling rig, a dynamic model for the ice, models for capturing the hydrodynamic interactions between the ice and platform, as well as models for capturing the impact between the two. Each component is described separately in this section.

Drilling Rig

The model of a typical semisubmersible drilling rig is adopted in the present study to investigate glacial ice interactions and impact. The platform is previously studied both numerically and experimentally during the EXWAVE JIP [22]. It is a modern drilling rig with four columns and two pontoons. The platform is designed for extreme environmental condition and is a representative for drilling rigs used in the Barents sea.

Hydrodynamic properties of the semisubmersible are obtained from a WAMIT® [23] analysis (Figure 2) that is further imported into the SINTEF Ocean's time-domain simulation tool SIMO®/SIMA® [24]. The obtained numerical model is further validated carefully against the model tests. The model tests of the EXWAVE semi-submersible were conducted at SINTEF Ocean’s Basin during October 2015 with a 1:50 scaled model of the hull (Figure 1). The semi's main particulars are given in Table 1. All values given here are in full scale, unless otherwise noted.

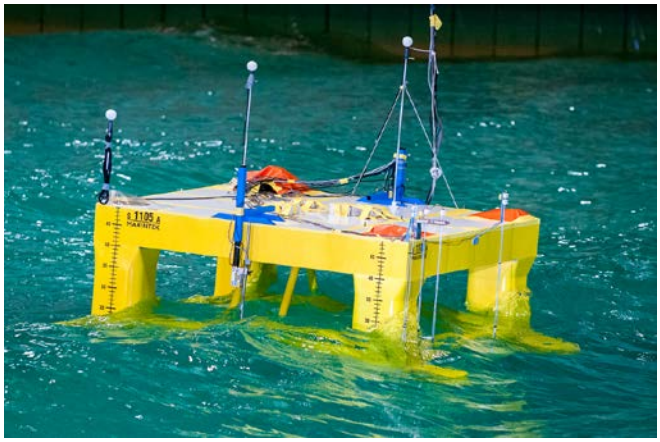

Figure 1. Photo showing the platform's model in the SINTEF Ocean's Ocean Basin.

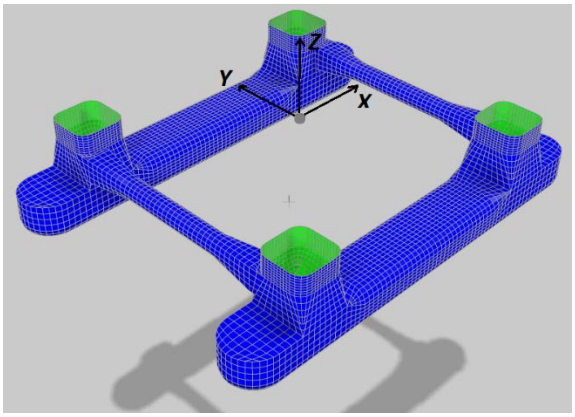

Figure 2. Surface model of the under-water part of the drilling rig prepared for WAMIT® calculations.

Table 1. Main particulars of the semi-submersible platform's model used in model tests.

Parameter	Model scale	Full scale
Length of pontoons	2.15 m	107.5 m
Breadth outside pontoons	1.625 m	81.25 m
Width of pontoons	0.2852 m	14.26 m
Height of pontoons	0.19 m	9.50 m
Width of columns	0.25 m	12.50 m
Breadth of columns	0.25 m	12.50 m
Long. dist. betw. columns	1.36 m	68.00 m
Trans. dist. betw. columns	1.34 m	67.00 m
Survival draft	0.46 m	23.0 m
Displacement	306 kg	39206 ton

Ice geometry and mass

Two different ice shapes are considered in this study: a prolate spheroid and a cuboid. Dimensions and mass for both shapes are presented in Table 2. These sizes are considered to be representative for the largest bergy bit which can approach floating units undetected. The shapes are selected to represent two different types: A round-shaped spheroid with a non-linear waterline, and a cuboid with sharp edges which ensures presence of viscous damping by enforcing flow separation.

Table 2. Shape, dimensions and mass of glacial ice

Spheroid	2c [m]	2a [m]	Mass [t]	Draft [m]
	15.0	10.4	765	8.1
Cuboid	**L [m]**	**H [m]**	**Mass [t]**	**Draft [m]**
	15.0	10.3	1432	9.0

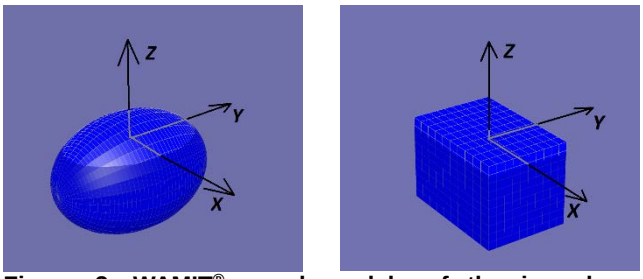

Figure 3. WAMIT® panel models of the ice shapes including definition of the local body coordinate systems: Spheroid (left) and cuboid (right).

The shapes are illustrated in Figure 3. The spheroid is characterized by the following equation:

$$\frac{X^2}{c^2}+\frac{Y^2+Z^2}{a^2}=1,$$

where c is the distance from center to the pole along the y-axis. The semi-axis a is the equatorial radius and the relationship to c is given as $a = 0.7c \cdot \exp(-0.00124c)$.

The cuboid is defined with its length L, height H and breadth B, and the relations are defined as H=B and $H = 0.7L \cdot \exp(-0.00124L)$.

Ice Dynamic

The dynamic model of ice is constructed based on decomposition of forces, rooted in linear assumption (see [24] and [25] for more details). The following components are considered with this respect:

- **Mass forces:** A mass matrix is calculated for the selected ice geometries, assuming uniform density of ice.
- **Hydrostatic forces:** Linear hydrostatic stiffness matrix, obtained from WAMIT®, is used in the linear calculations. This effect is directly included when nonlinear Froude-Krylov model is used, therefore the stiffness matrix is removed in those cases.
- **Potential flow radiation forces:** Radiation problem is solved using WAMIT® to calculate added mass and damping coefficients for the mean position of the ice. The results are transformed into retardation functions which is used by SIMO® to calculate radiation memory effects through convolution integrals.
- **Potential flow diffraction forces:** The forces acting on the ice due to diffracting the waves are calculated using WAMIT®. The Froude–Krylov component of the force is extracted, since it will be calculated separately.
- **Potential flow second order mean drift forces:** WAMIT® is also used to calculated drift coefficients for the mean position of the ice.
- **Potential flow, nonlinear, Froude-Krylov forces:** A model is developed and adopted to calculate underwater portion of the ice and the corresponding total

hydrostatic and hydrodynamic pressure at each time step. Forces, which included buoyancy and Froude-Krylov excitations are obtained by integrating pressure on the instantaneous wetted surface of the ice. The model is described in more details in the following text.

- **Viscous forces:** In order to model viscous forces a set of current coefficients, and slender elements with constant drag coefficients are adopted. The assumed net viscous drag forces, obtained from empirical drag coefficients found in [31], is decomposed into current coefficients, Morison-type element forces, and additional linear and quadratic damping coefficients in an attempt to represent a realistic approximation of the viscous forces. Due to nonlinearities involved, this decomposition is not entirely consistent. However, based on previous experience with tuning viscous forces on floating platforms, acceptable results are expected from this type of decomposition (e.g. [22]). In lack of model test data, this approach is considered to be the best available option for modelling the viscous forces, suitable for long time-domain simulations.

Six-degree-of-freedom model is used to solve the motions of the ice. Only wave interaction with ice is considered in the present study. Meaning current and wind forces are neglected. The stochastic waves are modelled using 3-parameter JONSWAP spectrum. The wave realization is obtained through Fourier analysis by selecting a seed number to present a random selection of phases for wave components.

During the simulation, the ice drift motion in the domain is considerable comparing to its length. Moreover, the correct phasing between the platform and ice motions is important for obtaining the point of impact. Therefore, the waves have to be calculated for the position of the ice, as it moves in the domain. Therefore, the Fourier wave components are transformed in time domain in order to include the phase shift in waves due to ice horizontal motions.

The ice has a density close to water. Therefore, it floats with small free-board and it can get fully submerged as it moves in waves. Moreover, the surface of the ice around the waterline is not necessarily vertical. A linear hydrostatic restoring, and Froude-Krylov excitation, model assumes that the ice surface is vertical around the water line, i.e. a constant waterplane area. This results in unrealistically large restoring forces when ice shapes with nonconstant waterplane area become submerged.

In the present study, the nonlinear Froude-Krylov force is calculated by obtaining the instantaneous underwater surface of the ice and integrating the incoming wave pressure on that. The free-surface elevation around the ice is reconstructed for a patch around the ice as shown in Figure 4. The ice surface is represented by triangles in a STL, stereolithography. The dynamic pressure due to incoming waves are constructed on a volume grid, starting from the mean free surface and extending downward, while it extends horizontally to the boundaries of the free-surface patch. The linear dynamic pressure is assumed constant above the mean water level. After cutting the ice geometry with instantaneous free surface to obtain the underwater surface, the hydro-static and dynamic pressures are calculated using the distance of the points from mean water surface, and interpolation of calculated dynamic pressures on the nodes of the volume grid.

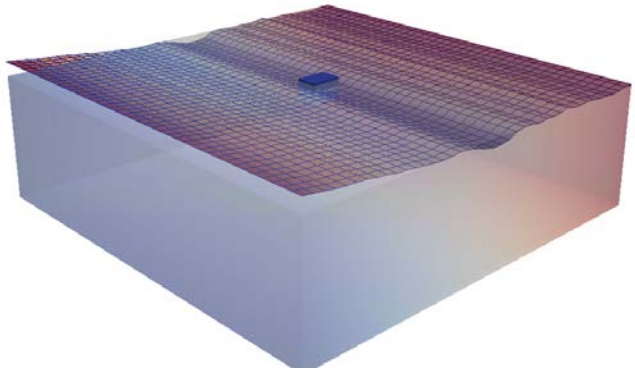

Figure 4. A view of the free surface patch and dynamic pressure box, with the ice in the center.

The horizontal extent of the free-surface patch and the dynamic pressure interpolation box are decided based on sensitivity studies. The surface patch and dynamic pressure box needs to be relocated and recomputed when the ice has drifted to the boundaries. On the other hand, selecting a too large domain put pressure on memory and slows down interpolation process at each time step. It is possible to optimize these parameters to achieve the best computation performance. Number of cells in these domains dictates the minimum resolvable wave length. This means prior to computations a cut-off frequency for the wave energy must be assumed. For most computations presented here, the elements sizes are chosen to be between 2 to 4 meters. This makes the shortest resolvable wave to be around 2 seconds.

A fixed ice cube in regular waves of 9.8[m] height and 14.8[s] period, traveling towards positive x-axis along the cube, is considered. The goal is to compare the obtained vertical force from different methods, i.e. linear, nonlinear Froude-Krylov (NLFK), and CFD, to see if the implemented model improves the linear predictions. In addition, it would be possible to verify the selected drag coefficients and the obtained viscous forces.

Figure 5 shows the comparison between vertical forces acting on a fixed ice from linear, NLFK, and CFD calculations. The linear model predicts a sinusoidal force as expected, while the NLFK model shows a very different behavior when the ice cube becomes submerged. The resulted force in this case is close to CFD but still missing the higher harmonic components, and viscous effects. Figure 6 shows a similar comparison when the viscous forces are included using a Morison-type elements forces and a constant drag coefficient. The viscous force is only included in the NLFK model. The obtained improvement comparing to CFD calculations is clear. The introduced viscous drag model here is further used in simulations of ice-platform impact.

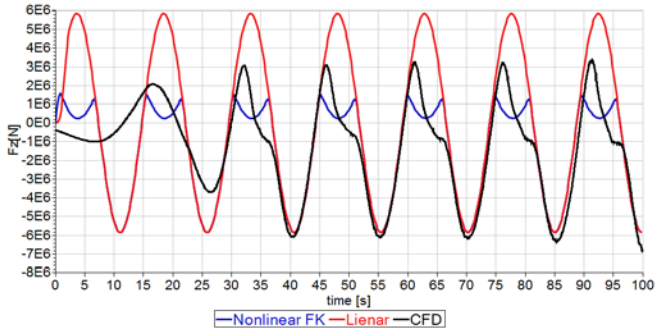

Figure 5. Vertical force acting on the fixed ice cube in regular waves of 9.8[m] height and 14.8[s] period from three different methods.

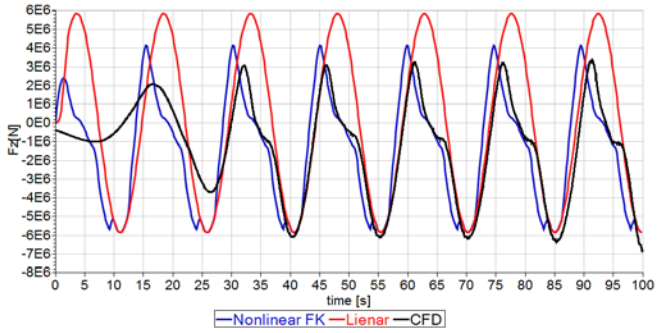

Figure 6. Vertical force acting on the fixed ice cube in regular waves of 9.8[m] height and 14.8[s] period from three different methods. Nonlinear FK model includes Morison-type viscous forces introduced through a slender element with constant drag coefficient.

Ice Impact

The dynamics of collision, e.g. crushing of ice during impact, are considered out of scope of the present study and not modelled. Therefore, the responses only up to the time of impact are considered and the rest neglected. The occurrence of impact between ice and platform is detected using bumper models in SIMO® [24]. The platform and ice are covered with cylindrical bumpers with spherical ends as shown in Figure 7. This will give the approximate boundaries of the selected platform and ice. Looking at the recorded bumper forces, the collision time is assumed to be the instance the bumper force becomes non-zero.

After determining the time of collision, the location and orientation of platform and ice are analyzed to determine the point of contact, and normal to the plane of contact. The ice and platform's STL geometries as well as the recorded response time series are used in the calculations (Figure 8). These calculations are done as a post-processing on the results after simulation.

Determining the normal of the contact plane, here referred to as *collision vector*, is particularly important for estimating the available kinetic energy during impact. The contact plane is defined as the plane in which the two bodies meet and transfer energy. Here it is assumed that this plane, and the collision vector, are constant during the impact. Moreover, the normal to the semi surface at the point of contact is assumed to be the collision vector ($\vec{n}_1$ in Figure 8). In addition, it is assumed that the available kinetic energy during impact can be calculated using the magnitude of relative velocity of semi and ice in the direction of the collision vector (u_{col}^2) as:

$$E = \frac{1}{2}(m_{ice} + A_{ice})u_{col}^2$$

where m_{ice} and A_{ice} are the ice mass and added mass in the direction of collision vector, respectively. This implies that both ice and semi stay intact during collision, and the ice velocity in the direction of collision vector will be equal to semi velocity in the same direction after the impact, which means that the ice will stick to the platform after impact, and any changes in the platform's velocity due to ice impact is neglected. The model also disregards the energy dissipation due to crushing of ice.

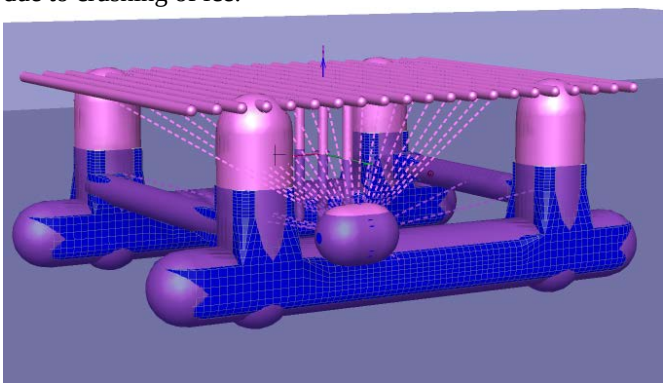

Figure 7. Schematic view of the bumper arrangement on the platform and ice. The dashed line connect the center points of all interacting bumpers.

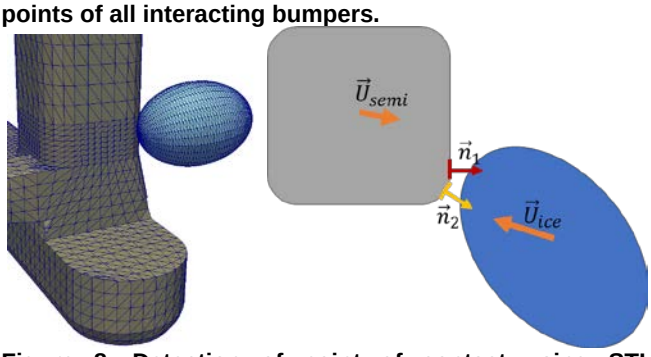

Figure 8. Detection of point of contact using STL geometries of platform and ice.

A conservative estimation of impact energy is expected to be obtained using this method. However, considering the crushing of ice can cause this estimation to be non-conservative due to change in the contact point and collision vector. This is particularly important when the impact happens around the corners, where the normal to semi surface is varying with location. Figure 8 shows a scenario where the contact point and collision vector can be changed from $\vec{n}_1$ to $\vec{n}_2$ when ice crushes. In this scenario, the magnitude of the relative collision velocity is larger in $\vec{n}_2$ direction, and hence a larger portion of the total kinetic energy of ice will be transferred to semi during impact. A model for crushing of ice is needed to assess the relative importance of above-mentioned increase in the impact energy and the energy loss due to crushing of ice.

Both zero and infinite frequency added mass at the time of impact could be used to calculate impact energy depending

on the impact process. If upon impact ice comes to abrupt stop then the infinite frequency added mass is an appropriate value. The infinite frequency implies that the water on the free-surface can move upward but has no time to propagate in the form of waves. This condition is mainly used in slamming models when the acceleration due to impact is dominant over the gravitation. On the other hand, if the ice quickly crushes during impact, and slowly stops after the impact, the zero-frequency condition, i.e. rigid free-surface, could be valid. Then the zero-frequency added mass is considered to give a better estimation of the kinetic energy at the time of impact.

Hydrodynamic interactions

Hydrodynamic interactions between ice and platform can change the response of the ice. Although the methodology developed here is designed to include these interactions, detailed investigations of these effects are left for future studies. Besides the motion of the ice, the interaction can change the ice added mass at the time of impact. This will influence the kinetic energy of the ice.

Figure 9 presents the variation of zero frequency added mass for the ice cube as it approaches the platform. The center of the ice cube, aligned with x-axis, is positioned at different locations around the platform and the zero-frequency added masses are calculated. Assuming rigid free-surface condition, i.e. slow motions of ice, the zero-frequency added mass is a representation of the ice added mass as it moves towards the platform. Let us assume the cube is simply drifting in x-axis towards the platform without any restoring. Then the motion can be formulated as,

$$(m + A_0)\ddot{\eta} + \dot{A}_0\dot{\eta} + B\dot{\eta} = F$$

Where, η is the ice's surge motion, m is the cube mass, A_0 is the zero-frequency added mass in surge, B is the damping coefficient in surge, F is the excitation force in surge, and upper dot represents time derivative. The term, $\dot{A}_0\dot{\eta}$, is introduced due to variation of added mass with time as ice approaches the platform. If $\dot{A}_0$ is positive, meaning the added mass is increasing, this would create a repellent force. Similarly, an attraction force can be expected when the ice moving away from the platform. This issue is studied before, for instance, in the scope of maneuvering of two interacting ships in [26]. To what extend this effect influence the motions of the ice, and how to include it for an object which oscillates in waves, needs further investigations. Here we make a brief attempt to partly include this effect in the present calculations.

The variation of added mass as the ice gets closer to the platform is considered for translational modes of ice, i.e. surge, sway and heave. The ice model presented before is modified by removing the convolution integrals in surge, sway and heave, and replacing it with the zero-frequency added mass in the respective modes, hence neglecting the memory effects in these modes of motions. The importance of including memory effects has been studied through sensitivity studies for these cases. It was concluded that beside the shortest wave condition studied here, the waves are long enough to allow for exclusion of memory effects. During time domain simulations, the zero-frequency added mass values of ice in surge, sway and heave, are extracted from the pre-calculated values shown in Figure 9, considering ice and semi locations, as well as ice orientation. Figure 10(top) shows how the surge and heave added mass of ice is changing in time for a scenario where the ice is drifting in the negative x-axis towards the column of the semi. In addition to changing the added mass value of ice, the forces due to variation of added mass in time, i.e. $-\dot{A}\dot{\eta}$, is calculated and included as excitation force in the dynamic equation of ice.

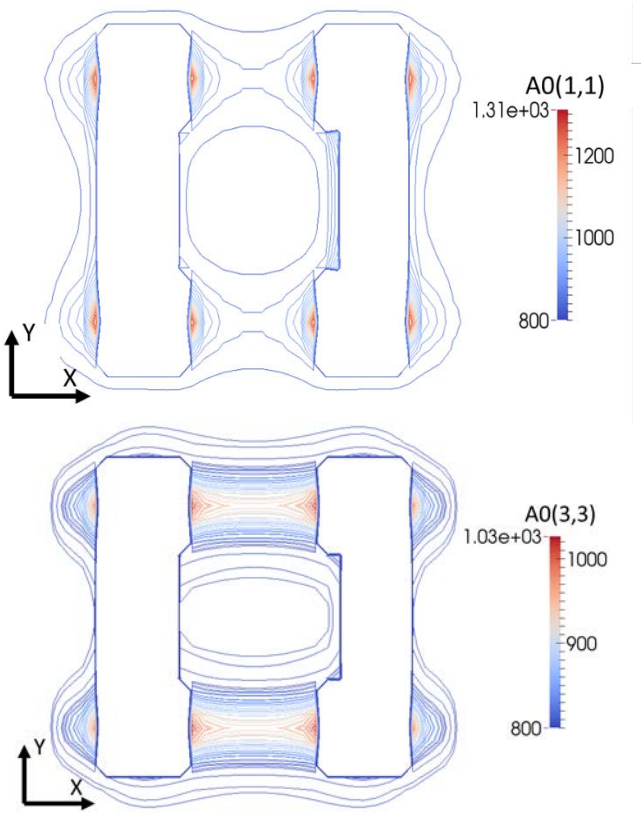

Figure 9. Zero frequency added mass [tons] of ice cube at different location around the platform. A0(1,1): ice added mass in surge, A0(3,3): ice added mass in heave. Platform pontoons are along x-axis. Ice cube length is along x-axis.

Figure 10(bottom) shows the obtained additional force due to variation of added mass in time until collision, and the comparison with the total excitation force in surge. It is clear that, in this case, the obtained repellent force at the time of impact is considerable comparing to the total excitation force. However, as will be discussed further in the following sections, the ice velocity at the time of impact is very sensitive to the initial conditions and selected seed for realizing irregular waves. Meaning, for a different seed number the repellent force at the time of impact could be negligible comparing to the total excitation force on the ice, mainly due to small surge velocity.

RESULTS AND DISCUSSIONS

The simulation results are presented here in terms of location and height of impact on the platform, and the

magnitude of relative collision velocity. The estimated impact energy of ice is also calculated and presented.

Selected cases

The selected environmental conditions for the present study are listed in Table 3, which consist of irregular waves only, i.e. current and wind are neglected. The stochastic waves are modelled using 3-parameter JONSWAP spectrum. The wave realization is obtained through Fourier analysis by selecting a seed number to present a random selection of phases for wave components. Only the one-year return period waves are selected from [21] and included in the present study.

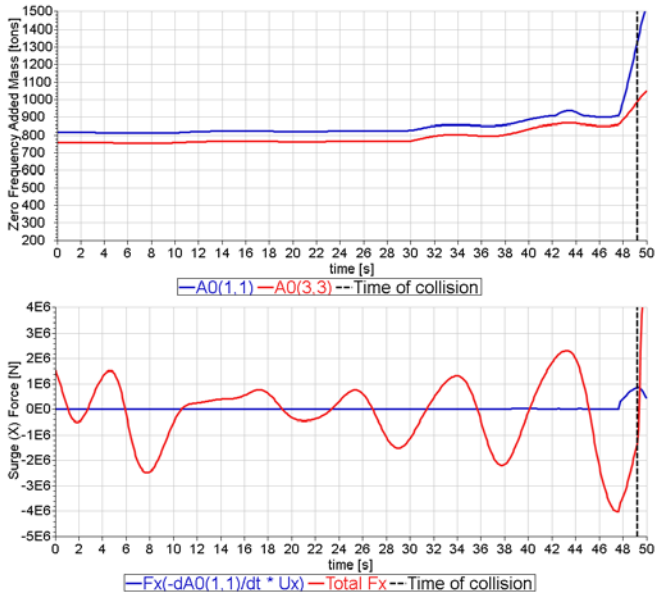

Figure 10. Top: Variation of ice added mass with time, A0(1,1): zero frequency ice added mass in surge, A0(3,3): zero frequency ice added mass in heave. Bottom: Excitation force due to variation of added mass, and total excitation force. The time of collision is shown with dashed line. Wave condition: Hs=9.8[m], Tp=14.8[s],wave direction = 180[deg]. Initial location of ice, X=70[m], Y=34[m]. Location of impact is column.

Table 3: Selected environmental conditions.

Enviroment ID (EID)	Tp [s]	Hs[m]	Gamma
1	14.8	9.8	1.4
2	12	8.6	2.9
3	6.5	4.9	5

The two ice geometries presented before are studied here, although the main focus is on the ice cube, where the geometry has been the center of validation and CFD studies. Figure 11 shows a schematic view of the initial locations and orientations of ice relative to platform, and the selected wave propagation directions. For the ice initial location to the right of the platform, i.e. positive x-axis, only the wave propagation along the x-axis is considered. The other wave propagation direction along y-axis is used with the initial ice locations above the platform, i.e. positive y-axis. The coordinates of the initial locations are listed in Table 4, while the platform's center is placed at the origin.

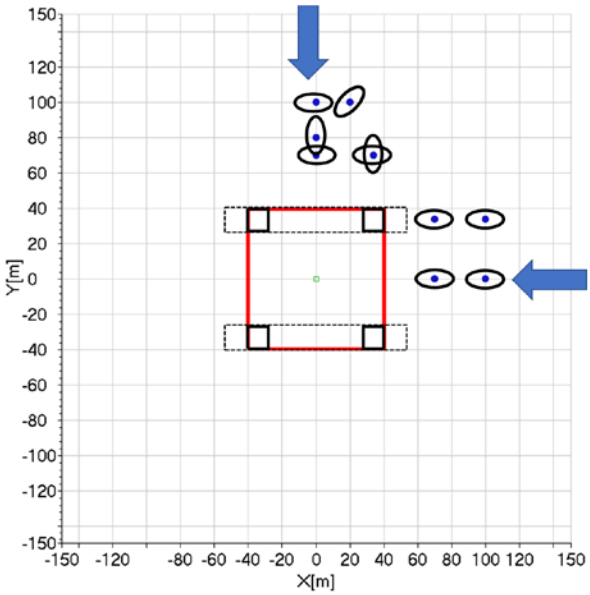

Figure 11. Schematic view of the platform and selected initial locations/orientations of ice. Blue dots show the center of ice, while the ellipse demonstrates the orientation. Blue arrows show the selected propagation directions for waves.

Table 4: Initial location and orientations of ice used in the present study, Rz: initial orientation of ice.

Location ID (LID)	X[m]	Y[m]	Rz[deg]
1	70	0	0
2	100	0	0
3	70	34	0
4	100	34	0
5	0	70	0
6	0	100	0
7	34	70	0
8	0	80	90
9	34	70	90
10	20	100	45

Each combination of location and environment is simulated for 20 different seeds. The number of seeds is increased to 40 in three cases and to 120 in a single case. In total 23 different cases have been considered. Results from a few cases are selected and discussed here. Table 5 shows the specification of the selected cases.

Height and location of impact

The results for impact location from all considered cases, are superimposed and presented in Figure 12. The main focus of impact points is on the column, mainly because in most of the simulations the ice is positioned on the path of collision to column (location 3,4,7, and 9). When the ice is positioned on the center line to the right of the platform, i.e. locations 1 and 2, it mainly hits the horizontal brace under the water which prevents it from coming in between the columns. When the ice is positioned above the platform on the center line, i.e. locations 5,6, and 8, the ice either hits the top surface of the pontoon or find its way in between the

columns and hit the inner cylinders which represent the risers.

Table 5. A selection of studied cases for column collision. Env. Cond. 1, i.e. Hs=9.8[m], Tp=14.8[s]. NLFK: nonlinear Froude-Krylov model, NLFK_A0: nonlinear Froude-Krylov model including the force due to variation of zero frequency added mass.

Case ID	Wave Direction [deg]	Num. Seeds	Method	Collision Location
Initial ice location (3): X= 70[m], Y=34[m], Rz=0[deg]				
1	180	20	NLFK	Column
2	180	20	NLFK_A0	Column
Initial ice location (8): X= 0[m], Y=80[m], Rz=90[deg]				
3	270	40	NLFK	Pontoon, Riser
4	270	120	NLFK_A0	Pontoon, Riser
5	270	40	NLFK_A0	Pontoon, Riser

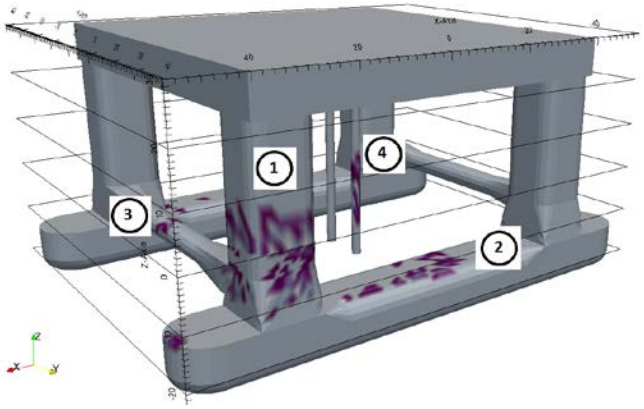

Figure 12. Superimposition of all collision points from the studied cases. The dark areas show the approximate collision location. The four collision locations selected for processing are marked with numbers, 1: Column, 2:Pontoon, 3:Brace, 4:Riser.

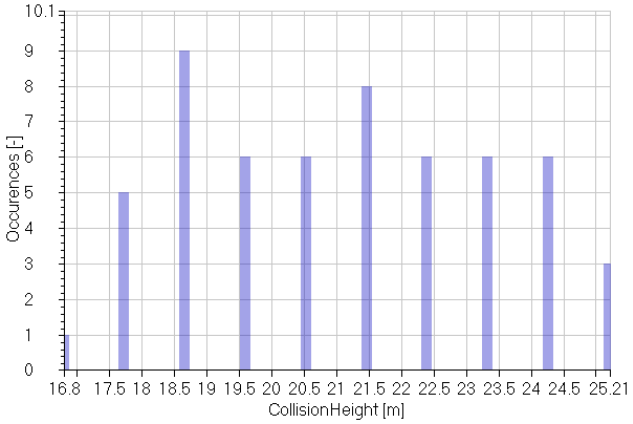

Figure 13. Distribution of collision height on risers for case 4, 56 different seeds, See Table 5 for more details. The collision height is measured from the bottom of semi, which is 23[m] below mean water line.

The statistics for the vertical location of impact on column and riser are presented for the selected cases in Table 6. The table also show the results of a Gumbel fit to the obtained values from different seed numbers. However, based on the distribution of impact height presented in Figure 13, it is clear that the application of the Gumbel distribution is questionable at best, and the model, even at 56 seeds, is not fully converged. Due to the complexity of the problem and dependency of the results to the details of the ice and semi motion, it is not possible to identify any clear trend in dependency of the height of impact to the studied wave conditions, or methods.

Table 6. Statistical values for vertical location of collision [m] for different scenarios (Table 5 and 6). The location is measured from the mean water level, i.e. Z=0. MP: Most probable, Exp: expected, P90: 90 percent fractal, based on a Gumbel fit.

Case ID	Max	Min	Mean	St. Dev.	MP	Exp	P90
Collision location: Column							
1	1.47	-10.19	-3.61	4.58	-5.71	-4.39	2.54
2	3.67	-10.19	-5.4	3.82	-7.17	-6.05	-0.22
Collision location: Risers							
3	3.33	-8.67	-1.79	3.09	-3.19	-2.3	2.32
4	2.67	-6.67	-1.89	2.47	-3.01	-2.3	1.36
5	2.67	-5.33	-2.55	1.98	-3.45	-2.88	0.09

Relative collision velocity

Table 7 shows the statistical values obtained for the relative collision velocity on the column, pontoon, and riser, for the relevant cases listed in Table 5. This velocity represents the relative velocity between the ice and platform at the time of impact. Figure 14 shows the distribution of the relative collision velocity on the column for case 1 with 20 seeds (see Table 5 for case details). Similar to the results of impact height, the Gumbel model is not converged here for 20 seeds due to large scattering of the occurrences, and its applicability is questionable. Moreover, it is not possible to identify any clear trend in the magnitude of the velocity at the time of impact based on the selected conditions. A set of simulations with many more seeds is desirable to address the statistical variability of the problem.

Table 7. Statistical values for relative collision velocity [m/s] for different scenarios (Table 5). MP: Most probable, Exp: expected, P90: 90 percent fractal, based on a Gumbel fit.

Case ID	Max	Min	Mean	St. Dev.	MP	Exp	P90
Collision location: Column							
1	3.9	0.38	1.66	1.1	1.15	1.47	3.13
2	2.64	0.14	1.07	0.65	0.77	0.96	1.95
Collision location: Riser							
3	2.46	0.21	1.27	0.49	1.04	1.18	1.92
4	3.54	0.24	1.53	0.71	1.21	1.41	2.46
5	2.57	0.4	1.4	0.61	1.13	1.3	2.21
Collision location: Pontoon							
3	1.82	0.08	0.92	0.53	0.68	0.83	1.65
4	3.42	0.03	1.01	0.68	0.7	0.9	1.91
5	2.01	0.07	1	0.6	0.72	0.89	1.8

Comparing the results for cases 1 and 2 in Table 7 shows the influence of introducing the force due to added mass variation on the relative collision velocity. A direct comparison of the two case suggests that the obtained repellent force decreases the expected collision velocity. However, it is important to note the strong dependency of

the results to the studied samples and the need for studying a larger number of seeds.

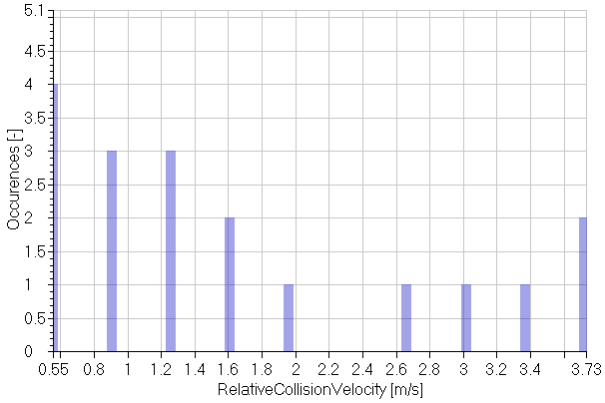

Figure 14. Distribution of relative collision velocity of the column for case 1. See Table 5 for more details.

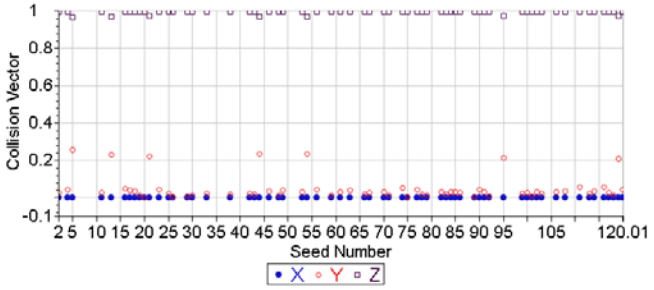

Figure 15. Components of collision vector, to the pontoon for different seeds in case 4. See Table 5 for more details.

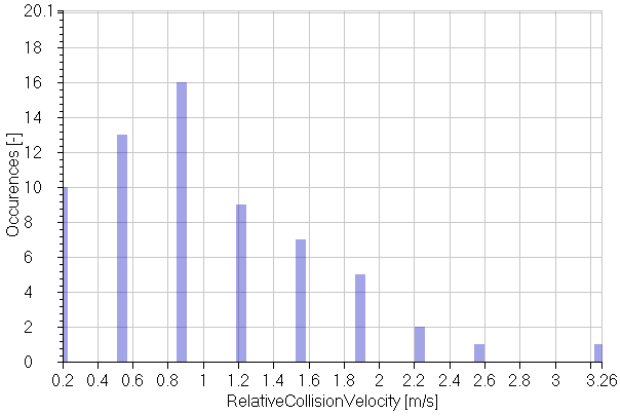

Figure 16. Distribution of relative collision velocity on the pontoon from case 4 with 64 seeds. See Table 5 for more details.

Figure 15 shows the collision vector components for 64 seeds out of 120 from case 4, where ice collides with the pontoon. The vertical components of collision vector (Z-component) is almost one in all the cases, suggesting that the ice hits the pontoon from the top in a vertical motion. Therefore, the relative collision velocity is mainly the relative vertical velocity of the ice and platform. As expected, the magnitude of relative collision velocity is smaller than the magnitude of ice total translational velocity, suggesting that only a portion of the total ice kinetic energy will contribute to the impact.

Comparing the results for case 3 and 4 in Table 7, which uses the same setup but different calculation method, suggests considering the variation of added mass as the ice gets closer to the platform increases the relative collision velocity. This is opposite of what has been observed for collision on the column. However, the collision vector, and hence the ice's mode of motion which contributes to the collision, is different in the two cases, i.e. one is surge, and the other is heave. The fact that only variation of heave added mass due to horizontal location of ice is included may be a factor as well. Figure 16 shows relative collision velocity distribution for case 4 with 120 seeds, where 64 out of 120 seeds result in pontoon collision and hence reported here. The comparison of this distribution to the one presented in Figure 14 suggests that increasing the number of seeds could improve the validity of Gumbel fit.

Kinetic energy at the time of impact

An estimation of the impact energy of the ice cube, with the mass of 1432 tons, is presented in Table 8, for collision on the column, riser, and pontoon. The statistical values, i.e. samples max and mean, as well as Gumbel estimations, for relative collision velocity are used in the calculations. As mentioned before, added mass values are affected by the presence of the platform. Moreover, the applicability of zero or infinite frequency added mass in this case depends on the speed of collision and solidity of ice. Here, the relevant zero-frequency added mass, considering the proximity effect, and the collision direction, is adopted in the calculations, which is a conservative approach to selecting the infinite-frequency added mass.

In all the cases considered here, the ice, when placed transverse to the waves, rotates and aligns itself with the waves before collision. Therefore, it is assumed that the collision is always happening in the longitudinal direction of ice, and hence the surge added mass is used in all horizontal collisions. When the collision vector is vertical, e.g. on the pontoon, then the heave zero-frequency added mass is adopted.

Table 8: Estimated impact energy [MJ] for the ice cube. The ice's zero-frequency added mass close to the platform is used in the calculations. MP: Most probable, Exp: expected, P90: 90 percent fractal, based on a Gumbel fit to relative collision velocities.

Case ID	Sample Mean	Sample Max	MP	Exp	P90
Collision location: Column ($A0_{11}$ = 1350[t])					
1	3.8	21.2	1.8	3.0	13.6
2	1.6	9.7	0.8	1.3	5.3
Collision location: Risers ($A0_{11}$ = 810[t])					
3	1.8	6.8	1.2	1.6	4.1
4	2.6	14.0	1.6	2.2	6.8
5	2.2	7.4	1.4	1.9	5.5
Collision location: Pontoon ($A0_{33}$ = 900[t])					
3	1.0	3.9	0.5	0.8	3.2
4	1.2	13.6	0.6	0.9	4.3
5	1.2	4.7	0.6	0.9	3.8

As expected, the obtained impact energies, similar to collision velocities, are highly dependent on the selected wave realization and initial conditions. Moreover, the

assumptions made for the impact process, mainly neglecting the crushing of ice during impact, will introduce inaccuracies in the present estimations of impact energy. A more complete impact solver, including models for ice crushing and hydrodynamic interaction during impact, is desirable. Then it would be possible to simulate the impact, starting from the ice and platform's velocities and positions at the time of impact, as identified here, and estimating the actual energy transfer between the two.

CONCLUSIONS AND FUTURE WORK

In the present paper, the behavior of smaller masses of glacial ice (less than 15 meters at the waterline, classified as growlers or bergy bits) in waves is studied through numerical simulations. The main objective was to assess the possibility of collision with non-enforced parts of a typical semisubmersible drilling unit. Moreover, to obtain a better understanding of the hydrodynamic interaction between glacial ice masses and semisubmersible drilling units and its importance for estimating collision energy.

The response of ice in waves is investigated using time-domain simulations and by partly introducing important nonlinear effects, in particular, nonlinear Froude-Krylov forces and the attraction/repellent force due to variation of zero-frequency added mass. Application of time-domain solution provided the possibility to introduce viscous effects and to investigate the sensitivity of the results to the waves sample variability.

It was shown that the nonlinear restoring and Froude-Krylov excitation forces are important due to large variation in the ice's waterplane area, and the fact that it can get completely submerged as it moves in waves. A nonlinear Froude-Krylov model is developed and validated against CFD, and previously existing model test data with reasonable accuracy. The CFD simulations is further used to validate a quadratic drag model for the ice cube, implemented using Morison drag forces. A clear improvement in the prediction of the vertical forces on the ice cube in regular waves was obtained using the developed model, in comparison to linear predictions.

A selection of irregular wave conditions, corresponding to one-year return period, is considered. Ten different initial locations and orientations of ice are investigated. The dependency of the results to selected realization of waves is investigated through seed variation. In total 23 different cases, 19 cases with 20 seeds, 3 with 40 seeds, and one with 120 seeds are studied. The simulations are processed until the first impact. Impact locations, ice and platform's velocities, collision vector, relative collision velocities, and estimated impact energies are presented.

Brief sensitivity study to the repellent/attractive force due to variation of zero-frequency added mass as the ice gets closer to the platform is presented. Strong dependency of the impact velocity and location to the ice initial location and selected wave realization is observed. Super imposing the collision locations for all considered realizations, it was clear that ice could impact the pontoons as well as the risers between the columns. Due to the large scatter of data it was not possible to conclude on any clear trend in the dependency of the impact results to the sea-state, initial ice location, or ice shape.

To calculate ice impact energy, suitable ice added mass is selected based on the collision vector and location. Moreover, most probable, expected and P90 fractal values for the magnitude of relative collision velocity are obtained by fitting a Gumbel distribution and presented, in addition to the recorded samples mean and absolute maximum. The expected impact energy is calculated using each of the statistical values of collision velocity; and presented for impact on column, pontoon, and riser separately. The dissipation of energy due to crushing of ice during impact is not considered in calculating the impact energy.

It was shown that the added mass at the time of impact varies based on the location of the ice. Moreover, how fast the ice is stopped after collision determines which added mass, i.e. zero or infinite frequency, is applicable. As a conservative measure, the larger of the two, i.e. zero-frequency added mass, is considered here. In addition, the variation of added mass as the ice approaches the column introduces a repelling force which is briefly studied for two of the cases considering only the translational motions of ice.

A more detailed study of nonlinearities in forces due to ice oscillations and its effect on the ice motion is of interest. Moreover, the influence of platform on the excitation and radiation forces of ice could be added in the next step. A more detailed investigation and validation of the implemented model for repelling/attracting forces is needed, in particular since these forces play an important role on determining the velocity of ice at the time of impact. The variability of the results with sea-state, wave realization, and ice location must be further studied through extensive sensitivity and seed variation investigations in an attempt to clarify the statistical behavior of the impact. Investigating existing, and novel, statistical models to represent this highly nonlinear process is of interest. Near-field description of ice mass collision with a steel hull needs to be further investigated in order to get a better understating of the impact energy. Such a study should include modelling of ice mechanics (crushing), deformation of hull, and the resulted variation of contact point and plane. In addition, comes the hydrodynamic interaction between the bodies during the collision.

ACKNOWLEDGEMENTS

We acknowledge The Norwegian Petroleum Safety Authority (Ptil) support of this study, especially Prof. Morten Langøy. Moreover, authors would like to thank Prof. Odd Faltinsen (NTNU) for the valuable discussions, and Dr. Reza Firoozkoohi (SINTEF Ocean) for contributions to the CFD calculations.

REFERENCES

[1] T. Sayeed, B. Colbourne, B. Quinton, D. Molyneux, H. Peng and D. Spencer, "A review of icebergs and bergy bit hydrodynamic interaction with offshore structures," *Cold Regions Science and Technology,* vol. 135, pp. 34-50, 2017.

[2] A. Tsarau, R. Lubbad and S. Løset, "Recent advances in modelling the hydrodynamic effects on ice motion and ice-structure interactions offshore," in *Proceedings of the 23rd International Conference on Port and Ocean Engineering under Arctic Conditions, (POAC15)*, Trondheim, Norway, 2015.

[3] V. M. Arunachalam, J. J. Murray and D. B. Muggeridge, "Short term motion analysis of icebergs in linear waves," *Cold Regions Science and Technology,* vol. 13, no. 3, pp. 247-2588, 1987.

[4] J. H. Lever and D. Sen, "A method to upgrade ice berg velocity statistics to include wave induced motion," *Journal of Offshore Mech. Arct. Eng.* , vol. 109, no. 2, pp. 278-286, 1987.

[5] J. H. Lever, B. Colbourne and L. Mak, "A model study of the wave-induced motion of small icebergs and bergy bits," *Journal of Offshore Mech. Arct. Eng.,* vol. 110, no. 1, pp. 101-107, 1988.

[6] J. H. Lever, D. Sen and D. Attwood, "The influence of shape on iceberg wave-induced velocity statistics," *Journal of Offshore Mech. Arct. Eng.,* vol. 112, no. 3, pp. 263-269, 1990.

[7] Hay and Company Consultants Inc, "Motion and impact of icebergs, Environmental studies revolvinng Funds report 004," Ottawa, 1986.

[8] M. Issacson and F. J. D. Stritto, "Motion of an ice mass near a large offshore structure," in *Offshore Technology Conference*, Houston, Texas, 1986.

[9] M. Isaacson and K. McTaggert, "Influence of hydrodynamic effects on iceberg collisions," *Can. J. Civ. Eng.,* vol. 17, no. 3, pp. 329-337, 1990.

[10] V. A. Chernetsov, A. A. Malyutin and S. L. Karlinsky, "Floating production platform for polar seas designed to resist iceberg impact," in *Proceedings of Eighteenth International Offshore and Polar Eng. Conf.*, 2008.

[11] S. L. Karlinsky and V. A. Chernetsov, "Floating production unit resistance to iceberg impact," in *Proceedings of the Twentieth International Offshore and Polar Engineering Conference*, 2010.

[12] S. G. Lee, I. H. Lee, Y. H. Baek, N. Couty, S. G. Geoff and J. M. Quenez, "Membrane-type LNG carrier side collision with iceberg - effect of impact conditions on structural respsonse through a sensitivity analysis," in *Presentated at 6th Ann Arctic Shipping Summit*, Helsinki, Finland, 2010.

[13] M. A. Salvaggio and M. Rojansky, "The importance of wave-driven icebergs impacting an offshore structure," in *Offshore Technology Conference*, Houston, Texas, 1986.

[14] L. M. Mak, J. H. Lever, M. J. Hinchey and D. Duthinh, "Wave-induced bergy bit motion near a floating oil production platform," in *Proceedings of the 9th International Conference on Offshore Mechanics and Arctic Engineering*, Houston, Texas, 1990.

[15] M. Isaacson and K. McTaggart, "Iceberg drift motions near a large structure," in *Proceedings of the First Pacific/Asia Offshore Mechanics Symposium*, Seoul, Korea, 1990.

[16] A. B. Cammaert and G. P. Tsinker, "Impact of large ice floes and icebergs on marine structures," in *Proceedings of the Sixth International Conference on Port and Ocean Engineering under Arctic Conditions*, Quebec, Canada, 1981.

[17] A. S. Swamidas, H. El-Tahan and M. Arockiasamy, "Structural integrity of semisubmersibles and gravity platforms to bergy-bit/iceberg impact," in *Offshore Technology Conference*, Houston, Texas, 1986.

[18] K. Holthe, "A numerical model for predicting the response of concrete gravity platforms to iceberg impact," in *Proceedings of the International Conference on Port and Ocean Engineering under Arctic Conditions*, Luleå, Sweden, 1989.

[19] Z. Liu and J. Amdahl, "A new formulation of the impact mechanics of ship collisions and its application to a ship-iceberg collision," *Marine Structures*, vol. 23, pp. 360-384, 2010.

[20] D. Bass, H. Gaskill and N. Riggs, "Analysis of iceberg impact with gravity base structures," in *Proceedings of the 4th International Conference on Offshore Mechanics and Arctic Engineering*, Dallas, Texas, 1985.

[21] DNVGL, "Ptil - Konstruksjonssikerhet i arktiske områder (ST5) - Glacial ice impact," Report No. 2017-0425, Rev. 2., March, 2018.

[22] N. Fonseca and C. Stansberg, "Wave drift forces and low frequency damping on the exwave semisubmersible," in *Proceedings of OMAE2017*, Trondheim, Norway, 2017.

[23] I. WAMIT, "WAMIT USER MANUAL Version 7.2," www.wamit.com, 2016.

[24] O. M. Faltinsen, Sea loads on ships and offshore structures, Cambridge, UK: Cambridge University Press, 1990.

[25] H. Ormberg, "SIMO Theory Manual V4.0, rev 1," MARINTEK, Trondheim, 2012.

[26] X. Xiang and O. M. Faltinsen, "Maneuvering of Two Interacting Ships in Calm Water," in *11th International Symposium on Practical Design of Ships and Other Floating Structures*, Rio de Janeiro, RJ, Brazil, 2010.

[27] J. H. Lever, D. Attwood and D. Sen, "Factors affecting the prediction of wave-induced iceberg motion," *Cold Regions Science and Technology,* vol. 15, pp. 177-190, 1988.

[28] D. Attwood, "Wave induced motions of small ice masses (Master thesis)," Memorial University of Newfoundland, 1986.

[29] K. F. Cheung, "Hydrodynamic interactions between ice masses and large offshore structures (Master thesis)," University of British Columbia, 1987.

[30] M. Isaacson and K. F. Cheung, "Influence of added mass on ice impacts," *Can. J. Civ. Eng.,* vol. 15, no. 4, pp. 698-708, 1988.

[31] D. J. McGovern and W. Bai, "Experimental study on kinematics of sea ice floes in regular waves," *Cold Regions Science and Technology,* vol. 103, pp. 15-30, 2014.

[32] R. D. Blevins, Applied Fluid Dynamics Handbook, Krieger Pub Co, 2003.